

---

# PRIVACY-PRESERVING LOW-RANK ADAPTATION FOR LATENT DIFFUSION MODELS

---

Zihao Luo<sup>1</sup>\*, Xilie Xu<sup>2</sup>\*, Feng Liu<sup>3</sup>, Yun Sing Koh<sup>1</sup>, Di Wang<sup>4</sup>, Jingfeng Zhang<sup>1,5†</sup>

<sup>1</sup>The University of Auckland

<sup>2</sup>The National University of Singapore

<sup>3</sup>The University of Melbourne

<sup>4</sup>King Abdullah University of Science and Technology

<sup>5</sup>RIKEN AIP

## ABSTRACT

Low-rank adaptation (LoRA) is an efficient strategy for adapting latent diffusion models (LDMs) on a training dataset to generate specific objects by minimizing the adaptation loss. However, adapted LDMs via LoRA are vulnerable to membership inference (MI) attacks that can judge whether a particular data point belongs to private training datasets, thus facing severe risks of privacy leakage. To defend against MI attacks, we make the first effort to propose a straightforward solution: privacy-preserving LoRA (PrivateLoRA). PrivateLoRA is formulated as a min-max optimization problem where a proxy attack model is trained by maximizing its MI gain while the LDM is adapted by minimizing the sum of the adaptation loss and the proxy attack model's MI gain. However, we empirically disclose that PrivateLoRA has the issue of unstable optimization due to the large fluctuation of the gradient scale which impedes adaptation. To mitigate this issue, we propose Stable PrivateLoRA that adapts the LDM by minimizing the ratio of the adaptation loss to the MI gain, which implicitly rescales the gradient and thus stabilizes the optimization. Our comprehensive empirical results corroborate that adapted LDMs via Stable PrivateLoRA can effectively defend against MI attacks while generating high-quality images. Our code is available at GitHub.

**Keywords** Latent diffusion models · privacy-preserving low-rank

## 1 Introduction

Generative diffusion models Ho et al. (2020); Song et al. (2020) are leading a revolution in AI-generated content, renowned for their unique generation process and fine-grained image synthesis capabilities. Notably, the Latent Diffusion Model (LDM) Rombach et al. (2022); Podell et al. (2023) stands out by executing the diffusion process in latent space, enhancing computational efficiency without compromising image quality. Thus, LDMs can be efficiently adapted to generate previously unseen contents or styles Meng et al. (2021); Gal et al. (2022); Ruiz et al. (2023); Zhang et al. (2023), thereby catalyzing a surge across multiple fields, such as facial generation Huang et al. (2023); Xu et al. (2024) and medicine Kazerouni et al. (2022); Shavlokhova et al. (2023).

Among various adaptation methods, Low-Rank Adaptation (LoRA) Hu et al. (2021) is the superior strategy for adapting LDMs. Compared to the full fine-tuning method that fine-tunes all parameters, LoRA not only requires less computational resources but also maintains commendable performance Cuenca & Paul (2023). Thus, LoRA enables individuals to adapt LDMs on small datasets or a series of private images using local machines Huggingface (2023).

However, recent studies Pang & Wang (2023); Dubiński et al. (2024); Duan et al. (2023) have pointed out that adapted LDMs via LoRA are facing the severe risk of privacy leakage. The leakage primarily manifests in the vulnerability to Membership Inference (MI) attacks Shokri et al. (2017), where sensitive information about the data used in the model's

---

\* Equal contribution.

† Correspondence to: Jingfeng Zhang <jingfeng.zhang@auckland.ac.nz>.

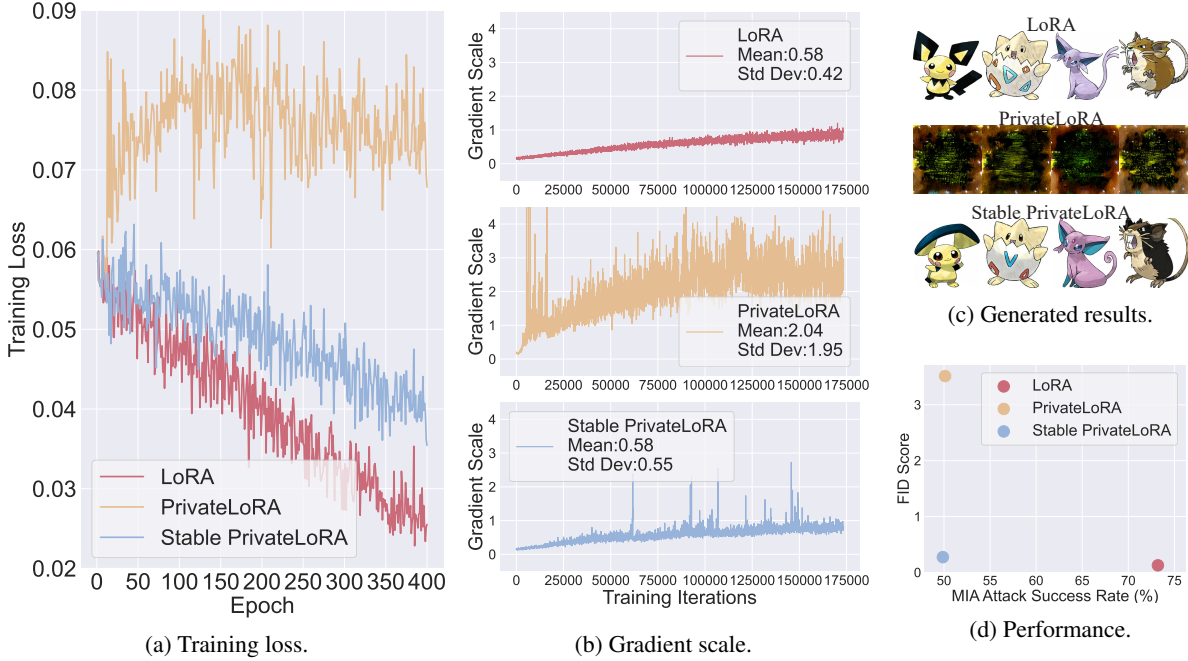


Figure 1: Figure 1a shows the trajectory of the training loss via LoRA, PrivateLoRA, and Stable PrivateLoRA on the Pokemon dataset. Figure 1b shows the mean value and standard deviation of gradient scales throughout the training iterations. Note that each epoch contains 433 training iterations. Figures 1c and 1d demonstrate the generated images and a comparison of evaluation metrics including FID Score and MI attack success rate (ASR). PrivateLoRA preserves membership privacy at the cost of diminished image generation capability. In contrast, Stable PrivateLoRA effectively preserves membership privacy while maintaining the quality of the generated image, demonstrating its effectiveness in defending against MI attacks without significant loss of functionality. Extensive generated images are visualized in Appendix A.7.

training process can be extracted. Generally, MI attacks utilize the model’s loss of a data point to differentiate whether it is a member of the training dataset or not. As shown in Figure 1d, adapted LDM via LoRA (red dot) exhibits an incredibly high Attack Success Rate (ASR) of 73.21%.

To mitigate the issue of privacy leakage, we make the first effort to propose a privacy-preserving LoRA (PrivateLoRA) method, which is formulated as a min-max optimization problem. Specifically, in the inner maximization step, a proxy attack model is trained to maximize its effectiveness in inferring membership which is quantitatively referred to as MI gain. In the outer minimization step, the LDM is adapted by minimizing the sum of the adaptation loss and the MI gain of the proxy attack model to enhance membership privacy-preserving.

However, PrivateLoRA encounters a significant issue in effectively optimizing the training loss, as evidenced in the orange line of Figure 1a. The potential reason could be the large and unstable fluctuation of the gradient scale during PrivateLoRA since the standard deviation of the gradient scale obtained by PrivateLoRA (the orange line in Figure 1b) is very high. This instability may hinder the convergence of the adapted LDM via LoRA Zhang et al. (2019), thus impeding optimizing the training loss.

To stabilize the optimization procedure of PrivateLoRA, we propose a Stable PrivateLoRA method, which incorporates the MI gain into the denominator of the adaptation loss instead of directly summing it. We theoretically show that this modification implicitly adjusts the gradient scale during adaptation, which can help to stabilize the gradient scale, as indicated by the similar means and standard deviation values of the gradient scale during Stable PrivateLoRA in blue lines of Figure 1b. Consequently, the mitigation of instability allows the adapted LDM via Stable PrivateLoRA to achieve better optimization, as shown in Figure 1a.

To evaluate the performance of the Stable PrivateLoRA, we conducted a series of adapting experiments using the Stable Diffusion v1.5 CompVis (2022) on the Pokemon Pinkney (2022) and CelebA Liu et al. (2015) datasets. Figure 1d shows that, although PrivateLoRA (orange dot) lowers the ASR to near-random levels, it significantly degrades the image generation capability of LoRA, as evidenced by a high FID score of 3.513 and the poor visual quality in Figure 1c. In

contrast, the Stable PrivateLoRA (blue dot) effectively preserves membership privacy without sacrificing generated image quality significantly, as evidenced by its FID score of 0.274 and ASR of 50.3%.

## 2 Background and Preliminaries

Here, we illustrate the related works and preliminaries regarding diffusion models, low-rank adaptation, as well as membership inference attacks.

### 2.1 Diffusion Model

Diffusion models (DMs) Ho et al. (2020); Song et al. (2020) have displayed remarkable performance in image synthesis. Compared with other generative models such as GAN Goodfellow et al. (2014), DMs can mitigate the problems of training instability and model collapse, while achieving state-of-the-art results in numerous benchmarks Dhariwal & Nichol (2021). Among the various implementations of DMs, the Latent Diffusion Model (LDM) is a noteworthy example. Fundamentally, LDM is a Denoising Diffusion Probabilistic Model (DDPM) Ho et al. (2020) built in the latent space, effectively reducing computational demand while enabling high-quality and flexible image generation Rombach et al. (2022). Therefore, LDMs have been widely utilized for adaptation Gal et al. (2022); Hu et al. (2021); Ruiz et al. (2023), capable of delivering high-performance models even when adapted on small datasets.

Adapting LDMs involves a training process that progressively adds noise to the data and then learns to reverse the noise, finely tailoring the model’s output. To be specific, an image  $x \in \mathcal{X}$  is initially mapped to a latent representation by a pre-trained encoder  $\mathcal{E} : \mathcal{X} \rightarrow \mathcal{Z}$ . In the diffusion process, Gaussian noise  $\epsilon \sim \mathcal{N}(0, 1)$  is progressively added at each time step  $t = 1, 2, \dots, T$ , evolving  $\mathcal{E}(x)$  into  $z_t = \sqrt{\alpha_t} \mathcal{E}(x) + \sqrt{1 - \alpha_t} \epsilon$ , where  $\alpha_t \in [0, 1]$  is a decaying parameter. Subsequently, the model  $f_\theta$  is trained to predict and remove noise  $\epsilon$ , therefore recovering  $\mathcal{E}(x)$ . Building on this, a pre-trained decoder reconstructs the image from the denoised latent representation. Furthermore, to incorporate conditional information  $y$  from various modalities, such as language prompts, a domain-specific encoder  $\tau_\phi$  is introduced, projecting  $y$  into an intermediate representation. Given a pair  $(x, y)$  consisting of an image  $x$  and the corresponding text  $y$ , the adaptation loss for LDM is defined as follows:

$$\ell_{\text{ada}}(x, y; t, \epsilon, f_\theta) = \|\epsilon - f_\theta(z_t, t, \tau_\phi(y))\|_2^2, \quad (1)$$

where  $\tau_\phi$  refers to the pre-trained text encoder from CLIP Radford et al. (2021).

### 2.2 Low-Rank Adaptation

As AI has recently shifted from universal models to adapted solutions, a variety of adaptation methods for LDMs have emerged. Low-Rank Adaptation (LoRA) Hu et al. (2021) provides an efficient and effective solution by freezing the pre-trained model weights and introducing the trainable low-rank counterparts, significantly reducing the number of trainable parameters and memory usage during the LoRA adaptation process. Therefore, LoRA not only lessens the demand for computational resources but also allows for the construction of multiple lightweight portable low-rank matrices on the same pre-trained LDM, addressing various downstream tasks Cuenca & Paul (2023); Huggingface (2023).

Specifically, when adapting LDMs via LoRA, a low-rank decomposition is performed on each attention layer in the LDM backbone  $f_\theta$ . During LoRA, assuming that the original pre-trained weight  $\theta \in \mathbb{R}^{d \times k}$ , a trainable LoRA branch  $\mathbf{BA}$  is randomly initialized and added to the pre-trained weights  $\theta$ , where  $\mathbf{B} \in \mathbb{R}^{d \times r}$ ,  $\mathbf{A} \in \mathbb{R}^{r \times k}$ . Note that the rank  $r$  is significantly less than  $d$  or  $k$ , which ensures the computational efficiency of LoRA. During the adaptation process via LoRA, for the augmented LDM backbone  $f_{\bar{\theta} + \mathbf{BA}}$ , all trainable LoRA branch parameters  $\mathbf{B}$  and  $\mathbf{A}$  are updated, while the original parameters  $\bar{\theta}$  are frozen. Given an image-test pair  $(x, y)$ , the adaptation loss during LoRA is formulated as follows:

$$\ell_{\text{ada}}(x, y; f_{\bar{\theta} + \mathbf{BA}}) = \|\epsilon - f_{\bar{\theta} + \mathbf{BA}}(z_t, t, \tau_\phi(y))\|_2^2. \quad (2)$$

For notational simplicity, we omit the variables  $t$  and  $\epsilon$  in the adaptation loss  $\ell_{\text{ada}}$ . Given the training dataset  $\mathcal{D}_{\text{tr}} = \{(x_i, y_i)\}_{i=1}^n$  composed of  $n \in \mathbb{N}^+$  image-text pairs, the training loss can be calculated as follows:

$$\mathcal{L}_{\text{ada}}(f_{\bar{\theta} + \mathbf{BA}}, \mathcal{D}_{\text{tr}}) = \frac{1}{n} \sum_{i=1}^n \ell_{\text{ada}}(x_i, y_i; f_{\bar{\theta} + \mathbf{BA}}). \quad (3)$$

Note that during the adaptation process via LoRA, the objective function that optimizes the parameters  $\mathbf{B}$  and  $\mathbf{A}$  is formulated as  $\min_{\{\mathbf{B}, \mathbf{A}\}} \mathcal{L}_{\text{ada}}(f_{\bar{\theta} + \mathbf{BA}}, \mathcal{D}_{\text{tr}})$ .

### 2.3 Membership Inference Attack

Membership inference (MI) attack Shokri et al. (2017) aims to determine whether specific data is part of a model’s training set. Recent studies Wu et al. (2022); Hu & Pang (2023); Matsumoto et al. (2023); Carlini et al. (2023); Pang et al. (2023); Duan et al. (2023); Kong et al. (2023) have shown that DMs are particularly vulnerable to MI attacks, thus undergoing high risks of privacy leakage.

As a pioneering work to research MI attacks on DMs, Wu et al. (2022) leveraged the intuition that when replicating training images, the model tends to produce images with a higher degree of fidelity and greater consistency with the corresponding textual captions. Based on this intuition, they conducted black-box attacks on text-to-image diffusion models at both pixel and semantic levels. Their findings revealed that the semantic-level attack outperformed the pixel-level attack with remarkable attack performance. To be more specific, by utilizing the pre-train BLIP model Li et al. (2022), a state-of-the-art vision-language model, to extract the embeddings of a given image and its corresponding caption-generated image, the semantic-level attack was then executed based on the distance between embeddings.

Meanwhile, for white-box attacks, Hu & Pang (2023) and Matsumoto et al. (2023) employed a threshold-based MI attack using the model loss at specific diffusion steps, as defined in Equation (1). This intuitive approach identifies training data by assessing whether the loss value falls below a certain threshold, demonstrating significant attack performance as well. These MI attacks have revealed that DMs are facing severe risks of privacy leakage.

To the best of our knowledge, no effective strategy has been proposed to protect membership privacy for adapted LDMs so far. Therefore, our paper takes the first step to propose an effective defence against MI attacks for DMs.

## 3 Stable Privacy-Preserving LoRA (Stable PrivateLoRA)

In this section, we first formulate the objective function of the min-max optimization problem for PrivateLoRA. Then, we disclose the unstable optimization issue of PrivateLoRA. Finally, we propose the Stable PrivateLoRA, as well as an algorithm for the specific implementation.

### 3.1 A Straightforward Solution: PrivateLoRA

**Objective function.** In MI attack, the conflicting objectives of defenders and adversaries can be modeled as a privacy game Shokri et al. (2012); Manshaei et al. (2013); Alvim et al. (2017). Adversaries can adjust their attack models to maximize MI gain against the target model, which requires that the defence can anticipate and withstand the strongest inference attacks. Consequently, the defender’s goal is to enhance membership privacy-preserving in worst-case scenarios where the adversary achieves the maximum MI gain while maintaining the model performance. Inspired by Nasr et al. (2018), we propose PrivateLoRA to defend against MI attacks which is formulated as a min-max optimization problem as follows:

$$\min_{\{\mathbf{B}, \mathbf{A}\}} \left( \underbrace{\mathcal{L}_{\text{ada}}(f_{\bar{\theta}+\mathbf{BA}}, \mathcal{D}_{\text{tr}})}_{\text{Adaptation loss}} + \underbrace{\max_{\omega} G(h_{\omega}, \mathcal{D}_{\text{aux}}, f_{\bar{\theta}+\mathbf{BA}})}_{\text{Membership inference gain}} \right), \quad (4)$$

where  $\mathcal{L}_{\text{ada}}(f_{\bar{\theta}+\mathbf{BA}}, \mathcal{D}_{\text{tr}})$  refers to the adaptation loss for the LDM with LoRA branch  $f_{\bar{\theta}+\mathbf{BA}}$  on the training dataset  $\mathcal{D}_{\text{tr}}$ ,  $h_{\omega}$  is the proxy attack model parameterized by  $\omega$ ,  $G(h_{\omega}, \mathcal{D}_{\text{aux}}, f_{\bar{\theta}+\mathbf{BA}})$  represents the MI gain of the proxy attack model  $h_{\omega}$  on the auxiliary dataset  $\mathcal{D}_{\text{aux}}$ .

Therein, the inner maximization aims to search for the most effective proxy attack model  $h_{\omega}$  for a given adapted LDM  $f_{\bar{\theta}+\mathbf{BA}}$  via maximizing the MI gain. The outer minimization, conversely, searches for the LDM  $f_{\bar{\theta}+\mathbf{BA}}$  that can best preserve membership privacy under the strong proxy attack model  $h_{\omega}$  while being able to adapt on the training dataset.

**Updating the proxy attack model in inner maximization.** The proxy attack model  $h_{\omega}$  equipped with white-box access to the target LDM  $f_{\bar{\theta}+\mathbf{BA}}$ , aims to infer whether a specific image-text pair  $(x, y)$  is from the training dataset  $\mathcal{D}_{\text{tr}}$  for adapting the target LDM  $f_{\bar{\theta}+\mathbf{BA}}$ . The model achieves this by constructing an auxiliary dataset  $\mathcal{D}_{\text{aux}}$ , which consists of half of the member data from  $\mathcal{D}_{\text{tr}}$ , denoted as  $\mathcal{D}_{\text{aux}}^m$ , and an equal amount of local non-member data  $\mathcal{D}_{\text{aux}}^{\text{nm}}$ . Using the auxiliary dataset  $\mathcal{D}_{\text{aux}}$ ,  $h_{\omega}$  trains a binary classifier based on the adaptation loss of target LDM  $f_{\bar{\theta}+\mathbf{BA}}$  to predict the probability of  $(x, y)$  for being a member of the  $\mathcal{D}_{\text{tr}}$ . Consequently, the MI gain of  $h_{\omega}$  can be quantified based on its

performance on the  $\mathcal{D}_{\text{aux}}$  as follows:

$$\begin{aligned} G(h_\omega, \mathcal{D}_{\text{aux}}, f_{\bar{\theta}+\mathbf{BA}}) = & \\ & \frac{1}{2|\mathcal{D}_{\text{aux}}^m|} \sum_{(x,y) \in \mathcal{D}_{\text{aux}}^m} \log(h_\omega(\ell_{\text{ada}}(x, y; f_{\bar{\theta}+\mathbf{BA}}))) \\ & + \frac{1}{2|\mathcal{D}_{\text{aux}}^{\text{nm}}|} \sum_{(x,y) \in \mathcal{D}_{\text{aux}}^{\text{nm}}} \log(1 - h_\omega(\ell_{\text{ada}}(x, y; f_{\bar{\theta}+\mathbf{BA}}))). \end{aligned} \quad (5)$$

In the inner maximization, the proxy attack model optimizes the parameters  $\omega$  by maximizing the MI gain, i.e.,  $\max_{\omega} G(h_\omega, \mathcal{D}_{\text{aux}}, f_{\bar{\theta}+\mathbf{BA}})$ .

**Adapting the LDM in outer minimization.** PrivateLoRA optimizes the LDM by directly minimizing a weighted sum of the MI gain of the  $h_\omega$  and the adaptation loss, which enables it to adapt to the training data and protect the private information of the training dataset simultaneously. To be specific, the training loss of PrivateLoRA is formulated as

$$\mathcal{L}_{\text{PL}} = \mathcal{L}_{\text{ada}}(f_{\bar{\theta}+\mathbf{BA}}, \mathcal{D}_{\text{tr}}) + \lambda \cdot G(h_\omega, \mathcal{D}_{\text{tr}}, f_{\bar{\theta}+\mathbf{BA}}), \quad (6)$$

where  $\lambda \in \mathbb{R}$  controls the importance of optimizing the adaptation loss versus protecting membership privacy. In the outer minimization of PrivateLoRA, the parameters  $\mathbf{B}$  and  $\mathbf{A}$  is updated by minimizing the  $\mathcal{L}_{\text{PL}}$ , i.e.,  $\min_{\{\mathbf{B}, \mathbf{A}\}} \mathcal{L}_{\text{PL}}$ .

PrivateLoRA is realized by one step of inner maximization to obtain a power proxy attack model by maximizing the MI gain in Equation (5) and one step of outer minimization to update  $\mathbf{A}$  and  $\mathbf{B}$  by minimizing the training loss in Equation (6). The algorithm of PrivateLoRA is shown in Algorithm 2 (Appendix A.2).

### 3.2 Issue of PrivateLoRA

Here, we empirically uncover that directly adding the MI gain into the objective function can prevent effectively optimizing the training loss (i.e.,  $\mathcal{L}_{\text{PL}}$ ). We collected and demonstrated the training loss at each training epoch in Figure 1a. The experimental details are illustrated in Section 4. Figure 1a shows that the PrivateLoRA's training loss (i.e., the sum of adaptation loss and the MI gain, shown as the orange line) does not gradually decrease as the training epoch increases. In contrast, the LoRA's training loss (i.e., the adaptation loss, shown as the blue line) can be well optimized. It indicates that introducing the term for protecting membership privacy (i.e., the MI gain) can impede the optimization procedure.

Next, we disclose that this optimization issue could be caused by the significant fluctuations in the gradient scale, especially obtained by the MI gain. We tracked and demonstrated the gradient scales of the training loss at each training iteration in Figure 1b. The training loss gradients w.r.t. parameters  $\mathbf{B}$  and  $\mathbf{A}$  during PrivateLoRA are calculated as follows:

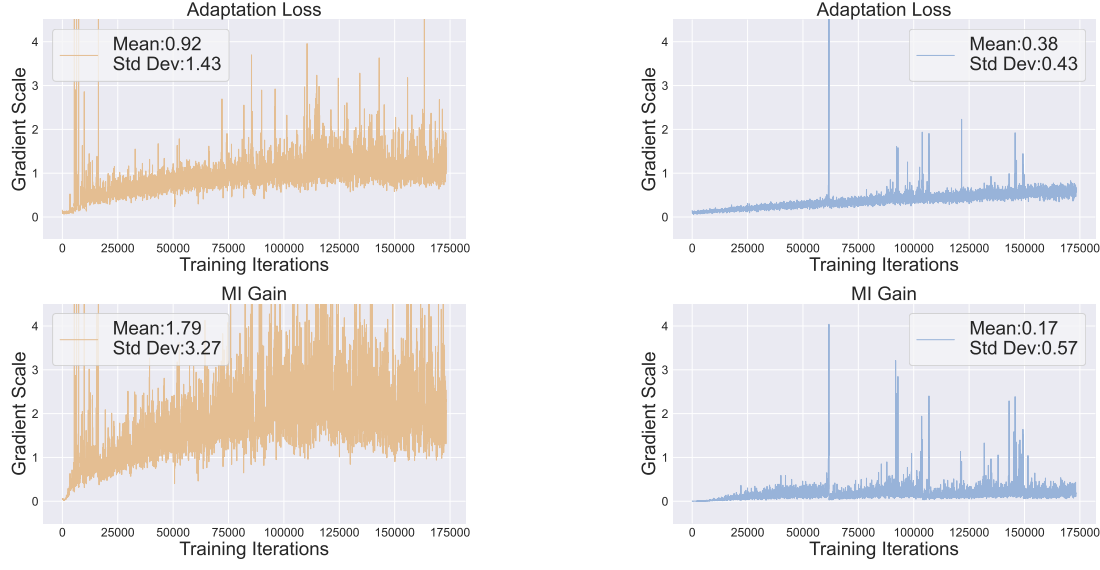
$$\begin{aligned} \frac{\partial \mathcal{L}_{\text{PL}}}{\partial \mathbf{B}} &= (\mu + \nu) \mathbf{A}^\top, \quad \frac{\partial \mathcal{L}_{\text{PL}}}{\partial \mathbf{A}} = \mathbf{B}^\top (\mu + \nu), \\ \text{where } \mu &= \frac{\partial \mathcal{L}_{\text{ada}}}{\partial \mathbf{BA}}, \quad \nu = \lambda \frac{\partial G}{\partial \mathbf{BA}}, \end{aligned} \quad (7)$$

in which  $\mathcal{L}_{\text{ada}}$  represents the adaptation loss and  $G$  represents the MI gain. Note that the gradient scale is calculated as the sum of the L2 norm of the gradients across all parameters in  $\mathbf{B}$  and  $\mathbf{A}$ , i.e.,  $\|\frac{\partial \mathcal{L}_{\text{PL}}}{\partial \mathbf{B}}\| + \|\frac{\partial \mathcal{L}_{\text{PL}}}{\partial \mathbf{A}}\|$ . Figure 1b shows that the standard deviation of gradient scales obtained by PrivateLoRA (1.95) is much higher than that obtained by LoRA (0.42). Such extremely unstable gradient fluctuation during PrivateLoRA can make the optimization more difficult and even fail Zhang et al. (2019).

Further, we analyze the gradient scales achieved by the adaptation loss and the MI gain during PrivateLoRA, which are calculated as  $\|\mu \mathbf{A}^\top\| + \|\mathbf{B}^\top \mu\|$  and  $\|\nu \mathbf{A}^\top\| + \|\mathbf{B}^\top \nu\|$  respectively, in Figure 2a. We observe that the standard deviation of the MI gain's gradient scale achieves 3.27, which is significantly higher than that achieved by the adaptation loss (1.43). Therefore, it suggests that the introduced MI gain that aims to protect privacy could be the primary cause of large fluctuations of the training loss gradient, which hinders the optimization and thus impedes the adaptation.

### 3.3 Stabilizing PrivateLoRA

To mitigate the aforementioned optimization issue of PrivateLoRA, we propose Stable PrivateLoRA by incorporating the MI gain into the denominator of the adaptation loss. The objective function of Stable PrivateLoRA is formulated as



(a) Gradient scale obtained by PrivateLoRA.

(b) Gradient scale obtained by Stable PrivateLoRA.

Figure 2: Tracking the gradient scale of the adaptation loss and the MI gain respectively for PrivateLoRA and Stable PrivateLoRA on the Pokemon dataset, based on Equation (7) and (10). For PrivateLoRA, the gradient scale of the MI gain exhibits a large standard deviation, which leads to the issue of effectively optimizing the training loss. In contrast, Stable PrivateLoRA has a more stable gradient scale for the MI gain, yielding a more stable optimization process.

follows:

$$\min_{\{\mathbf{B}, \mathbf{A}\}} \left( \frac{\mathcal{P}(f_{\bar{\theta}+\mathbf{B}\mathbf{A}}, \mathcal{D}_{\text{tr}})}{1 - \lambda \max_{\omega} G(h_{\omega}, \mathcal{D}_{\text{aux}}, f_{\bar{\theta}+\mathbf{B}\mathbf{A}})} \right). \quad (8)$$

To optimize Equation (8), Stable PrivateLoRA targets to minimize the following training loss function, i.e.,

$$\mathcal{L}_{\text{SPL}} = \frac{\mathcal{L}_{\text{ada}}(f_{\bar{\theta}+\mathbf{B}\mathbf{A}}, \mathcal{D}_{\text{tr}})}{1 - \lambda \cdot G(h_{\omega}, \mathcal{D}_{\text{tr}}, f_{\bar{\theta}+\mathbf{B}\mathbf{A}}) + \delta}, \quad (9)$$

where  $\delta$  is a stabilizer set at  $1 \times 10^{-5}$ , introduced to prevent the denominator from approaching zero and ensure stable calculation.

The specific implementation of Stable PrivateLoRA is detailed in Algorithm 1. At each training step, Stable PrivateLoRA will first update the proxy attack model by maximizing the MI gain and then update the LDM by minimizing the training loss  $\mathcal{L}_{\text{SPL}}$ .

Next, we provide a theoretical analysis to show that Stable PrivateLoRA can implicitly rescale the gradient, which helps mitigate the optimization issue. Note that the training loss gradient during Stable PrivateLoRA is calculated as follows:

$$\frac{\partial \mathcal{L}_{\text{SPL}}}{\partial \mathbf{B}} = (\mu' + \nu') \mathbf{A}^{\top}, \quad \frac{\partial \mathcal{L}_{\text{SPL}}}{\partial \mathbf{A}} = \mathbf{B}^{\top} (\mu' + \nu'), \quad (10)$$

where  $\mu' = \frac{1}{1 - \lambda G + \delta} \cdot \mu, \nu' = \frac{\mathcal{L}_{\text{ada}}}{(1 - \lambda G + \delta)^2} \cdot \nu,$

in which  $\mu$  and  $\nu$  are calculated in Equation (7). The detailed derivation is demonstrated in Appendix A.3. Then, the gradient scale obtained by the adaptation loss and the MI gain during Stable PrivateLoRA can be calculated as  $\frac{1}{1 - \lambda G + \delta} (\|\mu \mathbf{A}^{\top}\| + \|\mathbf{B}^{\top} \mu\|)$  and  $\frac{\mathcal{L}_{\text{ada}}}{(1 - \lambda G + \delta)^2} (\|\nu \mathbf{A}^{\top}\| + \|\mathbf{B}^{\top} \nu\|)$  respectively. Therefore, compared to PrivateLoRA, the gradient scales of the adaptation loss and the MI gain during Stable PrivateLoRA are implicitly rescaled by the factors  $\frac{1}{1 - \lambda G + \delta}$  and  $\frac{\mathcal{L}_{\text{ada}}}{(1 - \lambda G + \delta)^2}$ , respectively.

Observed from Figure 2, Stable PrivateLoRA obtains a much lower standard deviation of the gradient scale compared to PrivateLoRA. It indicates that the rescaling effect implicitly introduced by Stable PrivateLoRA can help stabilize the optimization, leading to a more stable gradient and controlled gradient scale. Zhang et al. (2019) has pointed out

**Algorithm 1** Stable PrivateLoRA

---

**Input:** Training dataset  $\mathcal{D}_{\text{tr}}$  for adaptation process, Auxiliary dataset  $\mathcal{D}_{\text{aux}} = \mathcal{D}_{\text{aux}}^{\text{m}} \cup \mathcal{D}_{\text{aux}}^{\text{nm}}$ , a pre-trained LDM  $f_{\theta}$ , a proxy attack model  $h_{\omega}$ , learning rate  $\eta_1$  and  $\eta_2$   
**Output:** a privacy-preserving adapted LDMs via LoRA  
 Perform low-rank decomposition on  $f_{\theta}$  to obtain  $f_{\bar{\theta}+\text{BA}}$

```

for each epoch do
  for each training step do
    Sample a batch  $S^{\text{m}}$  from  $\mathcal{D}_{\text{aux}}^{\text{m}}$ 
    Sample a batch  $S^{\text{nm}}$  from  $\mathcal{D}_{\text{aux}}^{\text{nm}}$ 
    Calculate MI gain  $G^* = G(h_{\omega}, S^{\text{m}} \cup S^{\text{nm}}, f_{\bar{\theta}+\text{BA}})$ 
    Update parameters  $\omega \leftarrow \omega + \eta_1 \cdot \nabla_{\omega} G^*$ 
    Sample a fresh batch from  $\mathcal{D}_{\text{tr}}$ 
    Calculate training loss  $\mathcal{L}^* = \mathcal{L}_{\text{SPL}}$ 
    Update parameters  $\mathbf{A} \leftarrow \mathbf{A} - \eta_2 \cdot \nabla_{\mathbf{A}} \mathcal{L}^*$ ,  $\mathbf{B} \leftarrow \mathbf{B} - \eta_2 \cdot \nabla_{\mathbf{B}} \mathcal{L}^*$ 
  end for
end for

```

---

that the gradient stability and controlled gradient scale facilitate faster and more reliable model convergence in the gradient descent of non-smooth and non-convex functions. Therefore, our proposed Stable PrivateLoRA is beneficial in improving the optimization convergence by implicitly stabilizing the gradient.

## 4 Experiment

In this section, we first evaluate the performance of LoRA, PrivateLoRA, and Stable PrivateLoRA in terms of image generation capability and effectiveness in defending against MI attacks. Then, we conduct ablation studies on the important hyperparameters and further evaluate the effectiveness of these methods in defending against MI attacks in the black-box setting Wu et al. (2022).

**Dataset.** In our experiment, we used two datasets: Pokemon Pinkney (2022) and CelebA Liu et al. (2015). We created two subsets based on the CelebA dataset, named CelebA\_Small and CelebA\_Large. The CelebA\_Small dataset consists of 200 images, from 25 randomly selected individuals, each providing 8 images. Similarly, the CelebA\_Large dataset contains 800 images from 100 randomly selected individuals. The Pokemon dataset contains text for each image which is generated by the pre-trained BLIP Li et al. (2022) model. For the CelebA\_Small and CelebA\_Large datasets, we also utilized the pre-trained BLIP model to generate corresponding text for each image.

For our experiments, each dataset was divided into four subsets:  $\mathcal{D}_{\text{aux}}^{\text{m}}$ ,  $\mathcal{D}_{\text{te}}^{\text{m}}$ ,  $\mathcal{D}_{\text{aux}}^{\text{nm}}$ , and  $\mathcal{D}_{\text{te}}^{\text{nm}}$ , with the detailed information provided in Table 5 (Appendix A.4). The dataset  $\mathcal{D}_{\text{tr}} = \mathcal{D}_{\text{aux}}^{\text{m}} \cup \mathcal{D}_{\text{te}}^{\text{m}}$  was used for adapting LDMs via LoRA. For PrivateLoRA and Stable PrivateLoRA, an additional dataset  $\mathcal{D}_{\text{aux}} = \mathcal{D}_{\text{aux}}^{\text{m}} \cup \mathcal{D}_{\text{aux}}^{\text{nm}}$  was utilized. To evaluate the effectiveness of adapted LDMs against MI attacks, we employed the data  $\mathcal{D}_{\text{te}} = \mathcal{D}_{\text{te}}^{\text{m}} \cup \mathcal{D}_{\text{te}}^{\text{nm}}$ .

**Model hyperparameters.** First, for adapting LDMs, we used the official pre-trained Stable Diffusion v1.5 CompVis (2022). The model hyperparameters, such as the rank  $r$  for LoRA and diffusion steps, are detailed in Table 6 (Appendix A.4). Second, the proxy attack model  $h_{\omega}$  is a 3-layer MLP with layer sizes [512, 256, 2], where the final layer is connected to a softmax function to output probability. Third, to evaluate the effectiveness of adapted LDMs in defending against MI attacks, we trained a new attack model  $h'$  on the auxiliary dataset  $\mathcal{D}_{\text{aux}}$  for 100 epochs. This model  $h'$ , structurally based on  $h$ , was then used to conduct MI attacks on the dataset  $\mathcal{D}_{\text{te}}$ . Both  $h_{\omega}$  and  $h'$  were optimized with the Adam optimizer with a learning rate of 1e-5. Furthermore, to prevent the attack model from being biased towards one side, we ensured that each training batch for both  $h_{\omega}$  and  $h'$  contained an equal number of member and non-member data points.

**Evaluation metrics.** To evaluate the effectiveness of PrivateLoRA and Stable PrivateLoRA in defending against MI attacks, we employed the following metrics: Attack Success Rate (ASR) Choquette-Choo et al. (2021), Area Under the ROC Curve (AUC), and True Positive Rate (TPR) at a fixed False Positive Rate (FPR) of 5% and 10%. The checkpoint of the  $h'$  with the highest ASR was identified as the point with maximum MI gain, and the corresponding AUC and TPR values were calculated. Lower values for ASR, AUC, and TPR indicate a more effective defence against MI attacks.

For assessing the image generation capability of the adapted LDMs, we utilized the Fréchet Inception Distance (FID) Heusel et al. (2017) scores and the Kernel Inception Distance (KID) Bińkowski et al. (2018) score for the

Table 1: Performance of LoRA, PrivateLoRA, and Stable PrivateLoRA across all three datasets, as measured by FID, KID, ASR, AUC, TPR at 5% FPR, and TPR at 10% FPR. Due to the limited size of the CelebA\_Small dataset, the FID scores are not available.

DATASET	METHOD	FID ↓	KID ↓	ASR (%) ↓	AUC ↓	TPR @5%FPR (%) ↓	TPR @10%FPR (%) ↓
POKEMON	LoRA	<b>0.127</b>	<b>0.0019</b>	74.1	0.79	3.43	28.76
	PRIVATELoRA	3.513	0.1237	<b>46.2</b>	<b>0.43</b>	<b>0.43</b>	<b>1.72</b>
	STABLE PRIVATELoRA	0.274	0.0048	50.3	0.58	0.86	6.44
CELEBA_SMALL	LoRA	N/A	0.056	94.0	0.97	92.0	94.0
	PRIVATELoRA	N/A	0.225	55.0	<b>0.41</b>	14.0	<b>14.0</b>
	STABLE PRIVATELoRA	N/A	<b>0.024</b>	<b>54.0</b>	0.54	<b>8.0</b>	16.0
CELEBA_LARGE	LoRA	<b>0.509</b>	<b>0.0553</b>	88.0	0.96	74.5	87.0
	PRIVATELoRA	3.759	0.2100	51.0	<b>0.51</b>	<b>1.0</b>	<b>6.5</b>
	STABLE PRIVATELoRA	0.556	0.0582	<b>50.0</b>	0.54	3.5	12.0

Pokemon and CelebA\_Large datasets. Specifically, the FID scores are calculated based on 768-dimensional feature vectors. For the CelebA\_Small dataset, which contains only 400 data points, we only calculated the KID scores. This is because we need the number of data points equal to or greater than the dimensions of the feature vector to ensure a full-rank covariance matrix for a correct FID score calculation. Lower values of FID and KID scores indicate better image quality and greater similarity between the generated and training images.

#### 4.1 Effectiveness of Stable PrivateLoRA in Defending against MI Attacks

In Table 1, we report the performance of LoRA, PrivateLoRA, and Stable PrivateLoRA, across the Pokemon, CelebA\_Small, and CelebA\_Large datasets. Compared to LoRA, PrivateLoRA displays considerably higher FID and KID scores, indicating lower quality of generated images. Meanwhile, PrivateLoRA exhibits near-random levels of ASR and AUC, along with low TPR values at both 5% and 10% TPR, showcasing its effectiveness in defending against MI attacks. This indicates that PrivateLoRA significantly enhances membership privacy but at the cost of image generation capability. Notably, the FID and KID scores for Stable PrivateLoRA closely align with those of LoRA, suggesting that Stable PrivateLoRA only makes a minor sacrifice to the quality of generated images. Also, Stable PrivateLoRA achieves near-random levels of ASR and AUC, and low TPR values at both 5% and 10% FPR. These results demonstrate that compared to PrivateLoRA, Stable PrivateLoRA effectively preserves membership privacy against MI attacks without significantly compromising image generation capability.

#### 4.2 Ablation Study

In this subsection, we conducted ablation studies on the important hyperparameters including the coefficient  $\lambda$  and the learning rate  $\eta_2$  that is used for updating the LDM’s parameters. Besides, we evaluated the effectiveness of Stable PrivateLoRA in preserving membership privacy under the MI attacks in the black-box setting Wu et al. (2022).

**Coefficient  $\lambda$ .** Tables 2 and 7 (Appendix A.5) present the performance of Stable PrivateLoRA with different coefficient  $\lambda \in \{1.00, 0.50, 0.10, 0.05, 0.01\}$  across the Pokemon, CelebA\_Small, and CelebA\_Large datasets. As  $\lambda$  decreases from 1.00 to 0.01, the FID and KID scores of Stable PrivateLoRA gradually decrease, indicating the higher quality of generated images. This trend occurs because, during the optimization of the training loss, a lower  $\lambda$  shifts the focus more towards minimizing adaptation loss, thus improving image generation capability. When  $\lambda = 0.01$ , both the ASR and AUC are greater than 0.5, indicating insufficient protection of membership privacy by Stable PrivateLoRA. Therefore, at  $\lambda = 0.05$ , we consider that Stable PrivateLoRA exhibits optimal performance for effectively preserving membership privacy at a minimal cost to image generation capability. For the experiments in Section 4.1 and subsequent ablation studies,  $\lambda$  is set at 0.05 for both PrivateLoRA and Stable PrivateLoRA.

Figure 3 and 4 (Appendix A.5) show the ROC curves for Stable PrivateLoRA with different  $\lambda$  values across all three datasets. We can observe that, in most cases, when  $\lambda \geq 0.05$ , Stable PrivateLoRA maintains a low TPR at 0.1%, 1%,

Table 2: The effect of coefficient  $\lambda$  for Stable PrivateLoRA on the Pokemon dataset. The results for the CelebA\_Small and CelebA\_Large datasets can be found in Table 7 (Appendix A.5).

$\lambda$	FID $\downarrow$	KID $\downarrow$	ASR (%) $\downarrow$	AUC $\downarrow$
1.00	1.633	0.0576	<b>46.0</b>	<b>0.42</b>
0.50	1.769	0.0694	46.2	0.46
0.10	0.361	0.0063	47.1	0.54
0.05	0.274	0.0057	50.3	0.58
0.01	<b>0.214</b>	<b>0.0048</b>	61.2	0.60

Table 3: The effect of learning rate  $\eta_2$  for Stable PrivateLoRA on the Pokemon dataset.

$\eta_2$	FID $\downarrow$	ASR (%) $\downarrow$	AUC $\downarrow$
1e-4	<b>0.274</b>	50.3	0.58
1e-5	0.436	46.2	<b>0.45</b>
1e-6	0.802	<b>45.9</b>	0.48

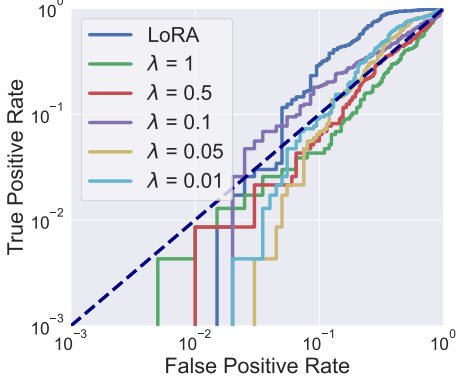


Figure 3: ROC curves for Stable PrivateLoRA with different  $\lambda$  on the Pokemon dataset.

Table 4: Performance of LoRA, PrivateLoRA, and Stable PrivateLoRA under MI attack in the black-box setting on the Pokemon dataset.

METHOD	ASR (%) $\downarrow$	AUC $\downarrow$
LoRA	72.4	0.67
PRIVATELoRA	<b>53.8</b>	<b>0.52</b>
STABLE PRIVATELoRA	55.4	0.54

and 10% FPR across all three datasets. These results demonstrate the effectiveness of Stable PrivateLoRA in defending MI attacks, whether under strict FPR constraints or more lenient error tolerance conditions.

**Learning rate  $\eta_2$ .** Table 3 displays the performance of Stable PrivateLoRA with different learning rates  $\eta_2 \in \{1e-4, 1e-5, 1e-6\}$  on the Pokemon dataset. We observe an increase in the FID scores as the learning rate  $\eta_2$  decreases. This phenomenon might be due to the lower learning rate resulting in the model being an underfitting state after 400 training epochs. Notably, regardless of the learning rate setting, Stable PrivateLoRA always preserves membership privacy, effectively defending against MI attacks.

**Defending against MI attacks in the black-box setting.** In Table 4, we report the attack performance of MI attacks on PrivateLoRA and Stable PrivateLoRA in a black-box setting Wu et al. (2022). Compared to LoRA, PrivateLoRA and Stable PrivateLoRA exhibit lower ASR and AUC, which indicates they can still effectively preserve membership privacy when facing MI attacks in the black-box settings. This black-box attack was replicated from the semantic-based Attack II-S proposed by Wu et al. (2022), with implementation details available in Appendix A.6.

## 5 Conclusion and Future Work

In this paper, we proposed privacy-preserving LoRA (PrivateLoRA), a method based on low-rank adaptation (LoRA) for adapting latent diffusion models (LDMs), while mitigating the risk of membership privacy leakage. We highlighted the issue in PrivateLoRA that directly minimizing the sum of the adaptation loss and MI gain can lead to large fluctuations in the gradient of MI gain, which results in unstable optimization. To address this issue, we proposed Stable PrivateLoRA, which implicitly rescales the gradient of MI gain by optimizing the ratios of the adaptation loss and the MI gain, thus stabilizing the optimization process. Comprehensive empirical results demonstrate that the adapted LDMs via Stable PrivateLoRA can effectively preserve membership privacy to defend against MI attacks while still generating high-quality images.

We propose three potential directions for the future work: 1). Investigating the performance of Stable PrivateLoRA under the gradient-based MI attacks Pang et al. (2023) in the white-box setting. 2). Exploring the application of the privacy-preserving method to other LDM adaptation methods such as DreamBooth Ruiz et al. (2023) and Textual Inversion Gal et al. (2022), to enhance membership privacy. 3). Developing more principled ways for selecting the coefficient  $\lambda$  value automatically rather than our current selection based on empirical observations.

## References

Alvim, M. S., Chatzikokolakis, K., Kawamoto, Y., and Palamidessi, C. Information leakage games. In *Decision and Game Theory for Security: 8th International Conference, GameSec 2017, Vienna, Austria, October 23-25, 2017, Proceedings*, pp. 437–457. Springer, 2017.

Bińkowski, M., Sutherland, D. J., Arbel, M., and Gretton, A. Demystifying mmd gans. *arXiv preprint arXiv:1801.01401*, 2018.

Carlini, N., Hayes, J., Nasr, M., Jagielski, M., Sehwag, V., Tramer, F., Balle, B., Ippolito, D., and Wallace, E. Extracting training data from diffusion models. In *32nd USENIX Security Symposium (USENIX Security 23)*, pp. 5253–5270, 2023.

Choquette-Choo, C. A., Tramer, F., Carlini, N., and Papernot, N. Label-only membership inference attacks. In *International conference on machine learning*, pp. 1964–1974. PMLR, 2021.

CompVis. Stable diffusion. <https://github.com/CompVis/stable-diffusion>, 2022. Accessed on January 16, 2024.

Cuenca, P. and Paul, S. Using lora for efficient stable diffusion fine-tuning, 2023. URL <https://huggingface.co/blog/lora>. Accessed on January 16, 2024.

Dhariwal, P. and Nichol, A. Diffusion models beat gans on image synthesis. *Advances in neural information processing systems*, 34:8780–8794, 2021.

Duan, J., Kong, F., Wang, S., Shi, X., and Xu, K. Are diffusion models vulnerable to membership inference attacks? *arXiv preprint arXiv:2302.01316*, 2023.

Dubiński, J., Kowalcuk, A., Pawlak, S., Rokita, P., Trzciński, T., and Morawiecki, P. Towards more realistic membership inference attacks on large diffusion models. In *Proceedings of the IEEE/CVF Winter Conference on Applications of Computer Vision*, pp. 4860–4869, 2024.

Gal, R., Alaluf, Y., Atzmon, Y., Patashnik, O., Bermano, A. H., Chechik, G., and Cohen-Or, D. An image is worth one word: Personalizing text-to-image generation using textual inversion. *arXiv preprint arXiv:2208.01618*, 2022.

Goodfellow, I., Pouget-Abadie, J., Mirza, M., Xu, B., Warde-Farley, D., Ozair, S., Courville, A., and Bengio, Y. Generative adversarial nets. *Advances in neural information processing systems*, 27, 2014.

Heusel, M., Ramsauer, H., Unterthiner, T., Nessler, B., and Hochreiter, S. Gans trained by a two time-scale update rule converge to a local nash equilibrium. *Advances in neural information processing systems*, 30, 2017.

Ho, J., Jain, A., and Abbeel, P. Denoising diffusion probabilistic models. *Advances in neural information processing systems*, 33:6840–6851, 2020.

Hu, E. J., Shen, Y., Wallis, P., Allen-Zhu, Z., Li, Y., Wang, S., Wang, L., and Chen, W. Lora: Low-rank adaptation of large language models. *arXiv preprint arXiv:2106.09685*, 2021.

Hu, H. and Pang, J. Membership inference of diffusion models. *arXiv preprint arXiv:2301.09956*, 2023.

Huang, Z., Chan, K. C., Jiang, Y., and Liu, Z. Collaborative diffusion for multi-modal face generation and editing. In *Proceedings of the IEEE/CVF Conference on Computer Vision and Pattern Recognition*, pp. 6080–6090, 2023.

Huggingface. Conceptual guides lora. [https://huggingface.co/docs/peft/conceptual\\_guides/lora](https://huggingface.co/docs/peft/conceptual_guides/lora), 2023. Accessed on January 16, 2024.

Kazerouni, A., Aghdam, E. K., Heidari, M., Azad, R., Fayyaz, M., Hacihaliloglu, I., and Merhof, D. Diffusion models for medical image analysis: A comprehensive survey. *arXiv preprint arXiv:2211.07804*, 2022.

Kong, F., Duan, J., Ma, R., Shen, H., Zhu, X., Shi, X., and Xu, K. An efficient membership inference attack for the diffusion model by proximal initialization. *arXiv preprint arXiv:2305.18355*, 2023.

Li, J., Li, D., Xiong, C., and Hoi, S. Blip: Bootstrapping language-image pre-training for unified vision-language understanding and generation. In *International Conference on Machine Learning*, pp. 12888–12900. PMLR, 2022.

Liu, Z., Luo, P., Wang, X., and Tang, X. Deep learning face attributes in the wild. In *Proceedings of International Conference on Computer Vision (ICCV)*, December 2015.

Manshaei, M. H., Zhu, Q., Alpcan, T., Bacşar, T., and Hubaux, J.-P. Game theory meets network security and privacy. *ACM Computing Surveys (CSUR)*, 45(3):1–39, 2013.

Matsumoto, T., Miura, T., and Yanai, N. Membership inference attacks against diffusion models. *arXiv preprint arXiv:2302.03262*, 2023.

Meng, C., He, Y., Song, Y., Song, J., Wu, J., Zhu, J.-Y., and Ermon, S. Sdedit: Guided image synthesis and editing with stochastic differential equations. *arXiv preprint arXiv:2108.01073*, 2021.

Nasr, M., Shokri, R., and Houmansadr, A. Machine learning with membership privacy using adversarial regularization. In *Proceedings of the 2018 ACM SIGSAC conference on computer and communications security*, pp. 634–646, 2018.

Pang, Y. and Wang, T. Black-box membership inference attacks against fine-tuned diffusion models. *arXiv preprint arXiv:2312.08207*, 2023.

Pang, Y., Wang, T., Kang, X., Huai, M., and Zhang, Y. White-box membership inference attacks against diffusion models. *arXiv preprint arXiv:2308.06405*, 2023.

Pinkney, J. N. M. Pokemon blip captions. <https://huggingface.co/datasets/lambdalabs/pokemon-blip-captions/>, 2022.

Podell, D., English, Z., Lacey, K., Blattmann, A., Dockhorn, T., Müller, J., Penna, J., and Rombach, R. Sdxl: Improving latent diffusion models for high-resolution image synthesis. *arXiv preprint arXiv:2307.01952*, 2023.

Radford, A., Kim, J. W., Hallacy, C., Ramesh, A., Goh, G., Agarwal, S., Sastry, G., Askell, A., Mishkin, P., Clark, J., et al. Learning transferable visual models from natural language supervision. In *International conference on machine learning*, pp. 8748–8763. PMLR, 2021.

Rombach, R., Blattmann, A., Lorenz, D., Esser, P., and Ommer, B. High-resolution image synthesis with latent diffusion models. In *Proceedings of the IEEE/CVF conference on computer vision and pattern recognition*, pp. 10684–10695, 2022.

Ruiz, N., Li, Y., Jampani, V., Pritch, Y., Rubinstein, M., and Aberman, K. Dreambooth: Fine tuning text-to-image diffusion models for subject-driven generation. In *Proceedings of the IEEE/CVF Conference on Computer Vision and Pattern Recognition*, pp. 22500–22510, 2023.

Shavlokhova, V., Vollmer, A., Zouboulis, C. C., Vollmer, M., Wollborn, J., Lang, G., Kübler, A., Hartmann, S., Stoll, C., Roider, E., et al. Finetuning of glide stable diffusion model for ai-based text-conditional image synthesis of dermoscopic images. *Frontiers in Medicine*, 10, 2023.

Shokri, R., Theodorakopoulos, G., Troncoso, C., Hubaux, J.-P., and Le Boudec, J.-Y. Protecting location privacy: optimal strategy against localization attacks. In *Proceedings of the 2012 ACM conference on Computer and communications security*, pp. 617–627, 2012.

Shokri, R., Stronati, M., Song, C., and Shmatikov, V. Membership inference attacks against machine learning models. In *2017 IEEE symposium on security and privacy (SP)*, pp. 3–18. IEEE, 2017.

Song, Y., Sohl-Dickstein, J., Kingma, D. P., Kumar, A., Ermon, S., and Poole, B. Score-based generative modeling through stochastic differential equations. *arXiv preprint arXiv:2011.13456*, 2020.

Wu, Y., Yu, N., Li, Z., Backes, M., and Zhang, Y. Membership inference attacks against text-to-image generation models. *arXiv preprint arXiv:2210.00968*, 2022.

Xu, J., Motamed, S., Vaddamanu, P., Wu, C. H., Haene, C., Bazin, J.-C., and De la Torre, F. Personalized face inpainting with diffusion models by parallel visual attention. In *Proceedings of the IEEE/CVF Winter Conference on Applications of Computer Vision*, pp. 5432–5442, 2024.

Zhang, J., He, T., Sra, S., and Jadbabaie, A. Why gradient clipping accelerates training: A theoretical justification for adaptivity. *arXiv preprint arXiv:1905.11881*, 2019.

Zhang, L., Rao, A., and Agrawala, M. Adding conditional control to text-to-image diffusion models. In *Proceedings of the IEEE/CVF International Conference on Computer Vision*, pp. 3836–3847, 2023.

## A Appendix

### A.1 Impact Statement

This paper proposes the Stable PrivateLoRA method, designed to enhance membership privacy protection for adapted Latent Diffusion Models (LDMs) via LoRA. This method is particularly valuable in the context of data-driven application scenarios, especially as AI shifts from universal models to adapted solutions, where safeguarding personal privacy becomes increasingly critical. While Stable PrivateLoRA firstly offers a powerful solution for adapting LDMs with privacy preservation, it's important to acknowledge the dual nature of its impact. On the one hand, Stable PrivateLoRA mitigates the risk of membership privacy leakage in adapted LDMs via LoRA. On the other hand, the general application and over-reliance on this method alone may lead to potential data misuse or inadvertently create gaps in overall data protection. Therefore, it is essential to recognize the need for a holistic approach to privacy protection, one that integrates Stable PrivateLoRA with multi-dimensional protection measures to ensure a comprehensive and responsible adaptation of LDMs.

### A.2 Algorithm of PrivateLoRA

We provide the specific implementation of PrivateLoRA as follows:

---

#### Algorithm 2 PrivateLoRA

---

**Input:** Training dataset  $\mathcal{D}_{\text{tr}}$  for adaptation process, Auxiliary dataset  $\mathcal{D}_{\text{aux}} = \mathcal{D}_{\text{aux}}^{\text{m}} \cup \mathcal{D}_{\text{aux}}^{\text{nm}}$ , a pre-trained LDM  $f_{\theta}$ , a proxy attack model  $h_{\omega}$ , learning rate  $\eta_1$  and  $\eta_2$

**Output:** a privacy-preserving adapted LDMs via LoRA

Perform low-rank decomposition on  $f_{\theta}$  to obtain  $f_{\bar{\theta}+\mathbf{BA}}$

**for** each epoch **do**

**for** each training step **do**

        Sample a batch  $S^{\text{m}}$  from  $\mathcal{D}_{\text{aux}}^{\text{m}}$

        Sample a batch  $S^{\text{nm}}$  from  $\mathcal{D}_{\text{aux}}^{\text{nm}}$

        Calculate MI gain  $G^* = G(h_{\omega}, S^{\text{m}} \cup S^{\text{nm}}, f_{\bar{\theta}+\mathbf{BA}})$

        Update parameters  $\omega \leftarrow \omega + \eta_1 \cdot \nabla_{\omega} G^*$

        Sample a fresh batch from  $\mathcal{D}_{\text{tr}}$

        Calculate training loss  $\mathcal{L}^* = \mathcal{L}_{\text{PL}}$

        Update parameters  $\mathbf{A} \leftarrow \mathbf{A} - \eta_2 \cdot \nabla_{\mathbf{A}} \mathcal{L}^*$ ,  $\mathbf{B} \leftarrow \mathbf{B} - \eta_2 \cdot \nabla_{\mathbf{B}} \mathcal{L}^*$

**end for**

**end for**

---

### A.3 Detailed Derivative Calculation for Equation (10)

We present the detailed steps for calculating the partial derivatives in Equation (10) w.r.t. parameters  $\mathbf{B}$  and  $\mathbf{A}$ .

$$\begin{aligned} \frac{\partial \mathcal{L}_{\text{SPL}}}{\partial \mathbf{B}} &= \frac{\partial \mathcal{L}_{\text{SPL}}}{\partial \mathbf{BA}} \cdot \frac{\partial \mathbf{BA}}{\partial \mathbf{B}} = \left( \frac{(1 - \lambda G + \delta) \frac{\partial \mathcal{L}_{\text{ada}}}{\partial \mathbf{BA}} - \mathcal{L}_{\text{ada}} \frac{\partial(1 - \lambda G + \delta)}{\partial \mathbf{BA}}}{(1 - \lambda G + \delta)^2} \right) \cdot \frac{\partial \mathbf{BA}}{\partial \mathbf{B}} \\ &= \left( \frac{1}{1 - \lambda G + \delta} \frac{\partial \mathcal{L}_{\text{ada}}}{\partial \mathbf{BA}} + \frac{\mathcal{L}_{\text{ada}}}{(1 - \lambda G + \delta)^2} \frac{\lambda \partial G}{\partial \mathbf{BA}} \right) \mathbf{A}^{\top}, \\ \frac{\partial \mathcal{L}_{\text{SPL}}}{\partial \mathbf{A}} &= \frac{\partial \mathcal{L}_{\text{SPL}}}{\partial \mathbf{BA}} \cdot \frac{\partial \mathbf{BA}}{\partial \mathbf{A}} = \left( \frac{(1 - \lambda G + \delta) \frac{\partial \mathcal{L}_{\text{ada}}}{\partial \mathbf{BA}} - \mathcal{L}_{\text{ada}} \frac{\partial(1 - \lambda G + \delta)}{\partial \mathbf{BA}}}{(1 - \lambda G + \delta)^2} \right) \cdot \frac{\partial \mathbf{BA}}{\partial \mathbf{A}} \\ &= \mathbf{B}^{\top} \left( \frac{1}{1 - \lambda G + \delta} \frac{\partial \mathcal{L}_{\text{ada}}}{\partial \mathbf{BA}} + \frac{\mathcal{L}_{\text{ada}}}{(1 - \lambda G + \delta)^2} \frac{\lambda \partial G}{\partial \mathbf{BA}} \right), \end{aligned}$$

where  $\mathcal{L}_{\text{ada}}$  represents the adaptation loss and  $G$  represents the MI gain.

#### A.4 Dataset and Model Hyperparameters

For our experiment setup, we provide detailed information on the division of datasets in Table 5 and model hyperparameters used for adapting LDMs via LoRA in Table 6.

Table 5: This table displays the sizes of the four subsets across all three datasets. The training dataset  $\mathcal{D}_{\text{tr}} = \mathcal{D}_{\text{aux}}^{\text{m}} \cup \mathcal{D}_{\text{te}}^{\text{m}}$  and the auxiliary dataset  $\mathcal{D}_{\text{aux}} = \mathcal{D}_{\text{aux}}^{\text{m}} \cup \mathcal{D}_{\text{aux}}^{\text{nm}}$  are utilized in the adaptation process for PrivateLoRA and Stable PrivateLoRA. The test dataset  $\mathcal{D}_{\text{te}} = \mathcal{D}_{\text{te}}^{\text{m}} \cup \mathcal{D}_{\text{te}}^{\text{nm}}$  is used to evaluate the effectiveness of PrivateLoRA and Stable PrivateLoRA in defending against MI attacks.

DATASET	$ \mathcal{D}_{\text{aux}}^{\text{m}} $	$ \mathcal{D}_{\text{te}}^{\text{m}} $	$ \mathcal{D}_{\text{aux}}^{\text{nm}} $	$ \mathcal{D}_{\text{te}}^{\text{nm}} $
POKEMON	200	200	200	233
CELEBA_SMALL	50	50	50	50
CELEBA_LARGE	200	200	200	200

Table 6: Hyperparameter settings for adapted LDM via LoRA. LoRA  $r$  is the rank used in the decomposition of the frozen weight matrix, as detailed in Section 2.2. LoRA  $\alpha$  is a scaling constant applied to the output of the LoRA branch **BA**.

MODEL	STABLE DIFFUSION V1.5		
LORA $r$	64	LORA $\alpha$	32
DIFFUSION STEPS	1000	NOISE SCHEDULE	LINEAR
RESOLUTION	512	BATCH SIZE	1
LEARNING RATE $\eta_1$	1e-5	LEARNING RATE $\eta_2$	1e-4
LEARNING RATE SCHEDULE	CONSTANT	TRAINING EPOCHS	400

#### A.5 Additional Results for Ablation Study

We provide the experiment results for the ablation study of coefficient  $\lambda$  on the CelebA\_Small and CelebA\_Large datasets. Table 7 reports the performance of Stable PrivateLoRA with different  $\lambda$ . Figure 4 shows the ROC curves of Stable PrivateLoRA with different  $\lambda$ . These results align with the conclusions drawn in the ablation study (Section 4.2).

Table 7: The effect of coefficient  $\lambda$  for Stable PrivateLoRA on the CelebA\_Small and CelebA\_Large dataset.

DATASET	$\lambda$	FID $\downarrow$	KID $\downarrow$	ASR (%) $\downarrow$	AUC $\downarrow$
CELEBA_SMALL	1	N/A	0.1867	54.0	0.54
	0.5	N/A	0.1004	<b>51.0</b>	<b>0.38</b>
	0.1	N/A	0.0592	55.0	0.54
	0.05	N/A	<b>0.0235</b>	54.0	0.41
	0.01	N/A	0.0545	78.0	0.85
CELEBA_LARGE	1	1.137	0.1116	52.0	0.48
	0.5	1.489	0.1559	52.8	0.51
	0.1	0.835	0.0767	<b>50.0</b>	<b>0.42</b>
	0.05	<b>0.556</b>	<b>0.0512</b>	<b>50.0</b>	0.54
	0.01	0.590	0.0582	57.3	0.58

#### A.6 Implementation of MI attacks in the black-box setting

In this section, we detail the implementation of the black-box MI attack used in Section 4.2. We replicate the semantic-based Attack II-S proposed by Wu et al. (2022). This attack leverages the pre-trained BLIP model to extract embeddings for an image and its corresponding text-generated image, and then conduct MI attacks based on the L2 distance between these two embeddings. Based on Wu et al. (2022)’s experiment setup, we instantiate this attack model as a 3-layer MLP, using cross-entropy as the loss function. It is optimized using the Adam optimizer with a learning rate of 1e-4 for 200 training epochs. The effectiveness of this attack against adapted LDMs via LoRA, PrivateLoRA, and Stable PrivateLoRA is presented in Table 4.

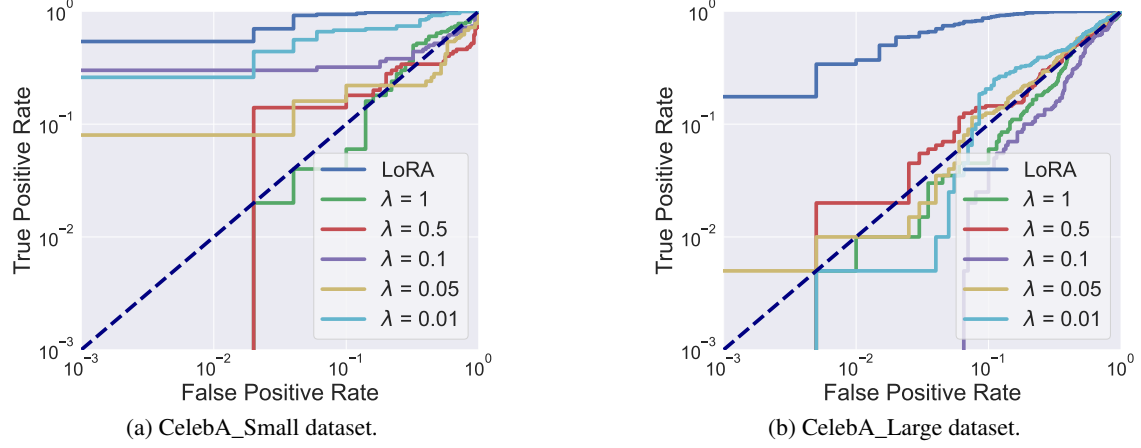


Figure 4: ROC curves for Stable PrivateLoRA with different  $\lambda$  on the CelebA\_Small dataset and CelebA\_Large dataset.

### A.7 Additional Generated Results

We provide more generated results of adapted LDMs via LoRA, PrivateLoRA, and Stable PrivateLoRA on the CelebA\_Small and CelebA\_Large datasets.



Figure 5: Generated results on the CelebA\_Small and CelebA\_Large datasets. Each column of three images is generated using the same text prompt.